

Level Set Simulations of Charged Droplets Using a Boundary Element Method

IEPC-2005-019

*Presented at the 29th International Electric Propulsion Conference, Princeton University
October 31 – November 4, 2005*

Anton VanderWyst*

University of Michigan, Ann Arbor, MI, 48109-2140 USA

Andrew Christlieb†

University of Michigan, Ann Arbor, MI, 48109-1043 USA

Mark Sussman‡

Florida State University, Tallahassee, FL 32306-4510 USA

Iain D. Boyd§

Univeristy of Michigan, Ann Arbor, MI 48109-2140 USA

Field emission electric propulsion (FEEP) thrusters are useful as μN , $\mu\text{-radian}$ attitude control devices for satellites due to their very high specific impulse. FEEP thrust can vary significantly depending on whether ions or droplets are emitted from the underlying needle. In this study, we simulate in planar 2D the emission of charged indium leaving the surface and forming independent droplets. The boundary element method is used to rapidly and accurately calculate the electric field on the fluid surface, which is then advected forward in time using the combined level set and volume of fluid (CLSVOF) method. The effects of surface tension, viscosity, electrode location and electrode potential on the formation of a droplet are analyzed. Variation of the size and charge of droplets at snapoff is presented.

*Graduate Research Assistant. Department of Aerospace Engineering. Email: antonv@umich.edu

†Assistant Professor. Department of Mathematics.

‡Assistant Professor. Department of Mathematics

§Professor. Department of Aerospace Engineering

Nomenclature

α	= source term for Neumann boundaries
d	= distance function for level sets
D	= rate of deformation tensor
$\partial_{\vec{n}}\{\}$	= vector normal derivative
$\vec{E}[\frac{V}{m}]$	= electric field
$\epsilon_0[\frac{F}{m}]$	= permittivity of free space
f	= Dirichlet boundary condition
F	= volume of fluid function
$\check{F}[\frac{N}{m^2}]$	= force per area on panels
g	= Neumann boundary condition
G	= Green's function
γ	= surface tension of liquid indium
$\check{\gamma}$	= source term for Dirichlet boundaries
h	= grid step size
H	= Heaviside step function
$\kappa[\frac{1}{m}]$	= surface curvature
$L[m]$	= panel length
$\mu[\frac{kg}{m \cdot s}]$	= liquid viscosity
\vec{n}	= vector normal
$N_D[\#]$	= number of Dirichlet boundary condition panels
$N_N[\#]$	= number of Neumann boundary condition panels
Ω	= surface
$\partial\Omega$	= surface boundary
$\partial\Omega_D$	= Dirichlet boundary
$\partial\Omega_N$	= Neumann boundary
p	= 2D pressure vector
ϕ	= level set, where $\phi = 0$ is the surface
$q[\#]$	= number of charges on panel
ρ	= fluid density
$\check{\rho}$	= areal charge density in fluid. Zero for perfect conductors
σ	= the mixed flux/potential variable solved for on the panel boundary
$\vartheta[\frac{m}{s}]$	= interface velocity
\vec{x}	= position vector $\begin{bmatrix} x \\ y \end{bmatrix}$
u, v	= x, y local velocities
$U(\vec{x})$	= potential at location \vec{x}
$\{\}_t$	= time change of [] vector
$\{\}_{x,y}$	= spatial change of [] vector

I. Introduction

Experimental efforts indicate that below a current of 20 μA , only ion emission occurs in FEEP needles.¹ Above that point, at a level that varies based on the thermal and electrical properties of the fluid, periodic stochastic motions of droplet formation and emission interrupt the steady ion stream. For the emitter to be an effective space attitude control thruster, a current of several hundred μA is necessary.² At such relatively large emissions, fluid instabilities occur and micro-droplets are emitted in addition to the ion current.^{3,4} The

existence and corresponding behavior of droplets is of large practical concern because as more droplets form, operational efficiency decreases, lifetime is limited and plume divergence is impacted due to non-identical charge distributions in the exhaust particles. Therefore, a numerical investigation into the formation and charge distributions among these expelled droplets is being undertaken.

The paper is organized as follows. Section I provides an overview of FEEP operation and utilization as a micro-Newton thruster. Section III presents the physical governing equations for the modeling. Section IV describes how the level set and boundary element methods solve these equations. Finally, Section V presents simulation results of physical parameter variation on droplet size and charge formation.

II. Field emitter description

In a field emitter, the surface of a conductive liquid is exposed to a strong electrostatic field which generates polarization forces. These forces move the liquid propellant in the field direction. As the potential on the ring electrodes increases, the surface liquid curvature increases until reaching a conical surface with a half angle of 49° , a so-called Taylor cone; this is where the forces of electrostatics and surface tension are mathematically in balance.⁵ A ring electrode with a -6 kV potential around a fine tungsten needle about 1 cm long and 1 mm thick accelerates the liquid metal indium, as represented in Fig. (1). The tip radius of needle curvature is on the order of $50 \mu\text{m}$ while the electrode is placed just a few mm above the droplet tip.

However, space charge effects near a fine point prevent full field evaporation. This effect can be avoided by allowing for a small jet above the underlying Taylor shape approximately 100 nm long and 30 nm in diameter.^{4,6,7} At this point, field emission occurs at the tip and along the rest of the surface. This behavior is well known in the literature.⁸⁻¹² When the field strength is on the order of $1 \frac{\text{V}}{\text{nm}}$, surface ions are field evaporated and rapidly accelerated past the electrodes to final velocities of upwards of 50 kilometers per second, producing thrust in the vacuum of space.

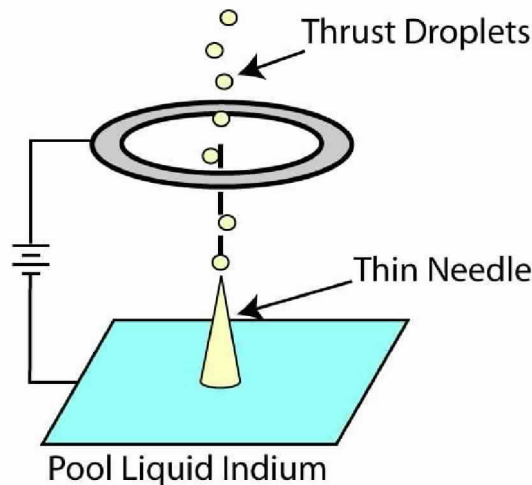


Figure 1. FEEP in droplet production mode

Field emission electric propulsion (FEEP) thrusters are currently being considered for a variety of space missions both in the United States and Europe. They offer very low thrust levels (μN), thrust repeatability ($<10 \text{ nN}$) and impulse bits ($\text{nN}\cdot\text{s}$) combined with a very high mass efficiency (8,000 seconds specific impulse). A similar technology is colloid thrusters, where organic propellant is substituted for indium and droplets are formed instead of the mixed regime. Both have been examined for decades^{13,14} and the ion/droplet plume composition has been formulated.^{15,16} Many scaling laws about current and voltage, droplet size and specific impulse have been published.¹⁷⁻¹⁹ Such thrusters are required for scientific drag-free missions such as LISA,²⁰ Darwin, GOCE²¹ and SMART-2. A space-tested indium FEEP has been under development for over a decade² and multiple thrusters in a cluster have been experimentally examined^{3,22} in Austria.

III. Model governing physical equations and justifications

The simulation model considers an incompressible, isothermal, viscous liquid. The propellant indium is treated as a perfect conductor. The two dimensional governing equations for a FEED are listed as Eqs. (1-4). The electric field is a surface normal force only, since \vec{E} is zero inside a conductor. Mass and momentum are conserved with Eq. (1).

$$\mathbf{A}_t + \mathbf{B}_x + \mathbf{C}_y = -\nabla p + \nabla^2 \mu \quad (1)$$

where the main variables are:

$$\mathbf{A} = \begin{bmatrix} \rho \\ \rho u \\ \rho v \end{bmatrix} \quad (2)$$

$$\mathbf{B} = \begin{bmatrix} \rho u \\ \rho u^2 \\ \rho uv \end{bmatrix}, \mathbf{C} = \begin{bmatrix} \rho v \\ \rho uv \\ \rho v^2 \end{bmatrix} \quad (3)$$

The electric field is computed with Poisson's equation, $\vec{E} = -\nabla U(\vec{x})$, where $U(\vec{x})$ is the electrostatic potential at position vector \vec{x} and u and v are local velocity vectors along the x and y axes. The free surface is advected with a pressure boundary condition.

$$p = \gamma\kappa + qE_n + 2\mu_{liquid}(D_{liquid} \cdot \vec{n}) \cdot \vec{n} \quad (4)$$

Interface curvature κ^{23} is a purely geometrically derived term and liquid rate of deformation tensor $D_{liquid} = \frac{1}{2}(\nabla \vec{x} + (\nabla \vec{x})^T)$.

The isothermal assumption primarily affects surface tension (γ) and viscosity (μ), for they are direct functions of the liquid temperature. Treating the surface tension of the fluid as a constant is reasonable as it varies minimally with temperature, as indicated by:²⁴

$$\gamma_{In} \left[\frac{N}{m} \right] = \frac{555 - 0.12(T[K] - 430)}{1000} \quad (5)$$

Indium's ability to flow over a surface is determined largely by its viscosity; using a constant value of flow resistance comes from noting viscosity changes with temperature as follows:²⁴

$$\mu_{In} \left[\frac{kg}{m \cdot s} \right] = 3 \times 10^{-4} e^{800/T[K]} \quad (6)$$

Between melting at 450 K and the normal operating temperature of 470K, the viscosity varies by only 8%, again validating the isothermal model assumption.

The assumption of a perfect conductor is also very reasonable. The imposition of mass conservation allows for the computation of indium velocity up the sides of the needle. As a metal, the conductivity of indium is so high that an electron can travel the fluid thickness in 6 ps while the fluid flows at a maximum speed of $100 \frac{\mu m}{s}$, or 10 orders of magnitude slower. An isothermal assumption is accurate because with only radiation to cool the droplets during the approximate 0.1 μs snap off, a 100 μm diameter droplet at 450 Kelvin cools 14 μK .²⁵

IV. Numerical methodology

When computationally tracking the movement of a surface between solid-liquid and liquid-vacuum interfaces using the equations of Sec. III, the calculation of the normal electric field \vec{E}_n often is quite drawn out and error-prone. However, Gibou presented an Eulerian approach to generate a symmetric, second-order accurate method with evenly spaced mesh points in an irregular domain to discretize the problem.²⁶ Another

approach is to combine level sets and the boundary element method to provide a rapid and equivalently accurate time simulation of field emitter droplet pinch-off.

The computational domain used in modeling the surface is the boundary element method (BEM), described below. The geometry of an axisymmetric slice through the needle is shown in Fig. (2).

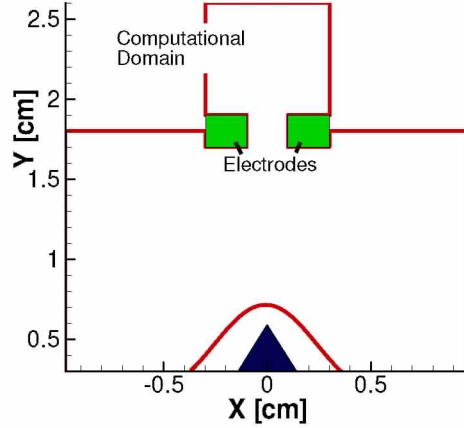


Figure 2. Simulation computational domain

The boundary bulge in the middle is meant to allow ions and droplets to propagate past the aperture and out into space. A flat no-flux Neumann boundary condition across the top center would mirror-reflect and flatten these droplets as they approached the electrodes from the needle surface.

A. Level set description

Interface tracking using level set computation relies on the determination and movement of the boundary from a fixed grid. Research has provided second-order accurate results on irregular domains. For FEEP operation, the indium propellant is adjacent to a hard vacuum. Figure (3) demonstrates that for any $\{x, y\}$ location there is a corresponding ϕ value associated with it. This is the level set function which is positive in liquid and negative in the vacuum. The $\phi = 0$ contour is the surface itself. Instead of front tracking, level sets change the values of ϕ at fixed locations in space and then recreate that zero crossing at each time step as the location of the surface moves in or outward. The position of the free surface is updated via the level set equation:

$$\phi_t + \vec{\vartheta} \cdot \nabla \phi = 0 \quad (7)$$

where $\vec{\vartheta}$ is the interface velocity, taken to be the fluid velocity for $\phi > 0$ and an extension of the fluid velocity for $\phi < 0$. Equation (7) states that ϕ remains constant on particle paths.

The curvature of the interface κ can then be described using the level set variable ϕ itself as

$$\kappa = \frac{\nabla \cdot (\nabla \phi)}{|\nabla \phi|} \quad (8)$$

The free surface is represented through a ‘‘coupled level set and volume-of-fluid’’ (CLSVOF) method. In addition to solving the level set equation (7), the volume-of-fluid function F is computed,²⁷ using

$$F_t + \vartheta \cdot \nabla F = 0 \quad (9)$$

where the net volume of fluid is conserved both in local cells and globally. Interfaces are tracked in this volume-of-fluid method by locally calculating the flux of volume in or out of a given computational cell. If a cell has no fluid, $F=0$; totally filled grid points have $F=1$. Interface (‘mixed’) cells have $F=(0,1)$.²⁸ The initial volume values are created using H , the Heaviside function evaluated at grid cells i, j in Eq. (10).

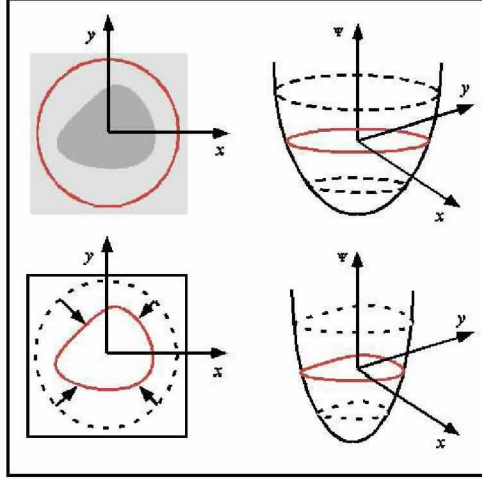


Figure 3. Level set hierarchy

$$F_{ij} = \frac{1}{\Delta x \Delta y} \int_{\Omega_{ij}} H(\phi(x, y)) \partial x \partial y \quad (10)$$

Using the above definitions for level sets, this work builds on prior two and three dimensional efforts of interface migration by Sussman.²⁹ However, the efficient calculation of the magnitude of the normal electric field $|\vec{E}_n|$ in Eq. (4) presents many challenges. A proposed algorithm for determining this electrostatic force is the boundary element method.

B. Boundary element method description

The boundary element method rapidly and directly solves for the force on the surface without meshing the volume of the domain. It handles arbitrary geometries by only discretizing points along the boundary. For example, consider Poisson's equation:

$$\Delta U(\bar{x}) = \frac{\check{\rho}}{\epsilon_0}, U|_{\partial\Omega} = f \text{ or } \nabla U|_{\partial\Omega} \cdot \vec{n} = g, \bar{x} \in \Omega \quad (11)$$

where $\check{\rho}$ is the charge density, f is the Dirichlet fixed-potential and g is the Neumann fixed-flux boundary condition and U is the potential. A solution to Poisson's equation can be formed using a Green's function approach.

1. Green's function

Let $G(\bar{x}|\bar{x}_0)$ be the free space Green's function for the Laplace operator, which is the solution to

$$\Delta G = \delta(\bar{x} - \bar{x}_0) \quad (12)$$

where $\bar{x} = (x, y)$ is a boundary point and \bar{x}_0 is a point on the interior of the domain. In two dimensional coordinates, the function becomes:

$$G = -\frac{1}{4\pi} \ln\{(x_0 - x)^2 + (y_0 - y)^2\} \quad (13)$$

Using Green's 2^{nd} identity:

$$\int \int_A (D \Delta E - E \Delta D) dA = \oint (D \nabla E - E \nabla D) \cdot \vec{n} dS \quad (14)$$

and replacing D by the Greens function G and E by U gives

$$\int \int_A G \frac{\check{\rho}(\bar{x})}{\epsilon_0} dA - U(\bar{x}_0) = \oint (G(\partial_{\vec{n}} U) - U(\partial_{\vec{n}} G)) \cdot \vec{n} dS \quad (15)$$

where $\partial_{\vec{n}} x = \nabla x \cdot \vec{n}$. Since we do not have any internal charge due to the assumption of a perfect conductor, $\check{\rho}(\bar{x}_0) = 0$ and the potential at any point can be calculated from the boundary flux and potential conditions alone. *Carefully* taking the limits of the single and double layered potential³⁰ gives the boundary integral formulation for Laplace's equation from the inside of the domain.

$$\frac{U(\bar{x}_0)}{2} = \oint_{\partial\Omega} U(\bar{x}) \partial_{\vec{n}} G(\bar{x}|\bar{x}_0) ds - \oint_{\partial\Omega} \partial_{\vec{n}} U(\bar{x}) G(\bar{x}|\bar{x}_0) ds \quad (16)$$

Here, $\partial\Omega$ consists of a mixture of $U(\bar{x})$ along $\partial\Omega_D$ and $\partial_{\vec{n}} U(\bar{x})$ along $\partial\Omega_N$ boundary conditions, where $\partial\Omega = \partial\Omega_D + \partial\Omega_N$.

2. Numerical discretization of the problem

Approximating the potential and flux of each panel as being a C_{-1} constant over the N_D Dirichlet and N_N Neumann panels along surface ds gives:

$$\begin{aligned} \oint_{\partial\Omega_D} U(\bar{x}) \partial_n G(\bar{x}|\bar{x}_0) ds &\approx \sum_{i=1}^{N_D} U(\bar{x}_i) \oint_{\partial\Omega_{D,i}} \partial_n G(\bar{x}|\bar{x}_0) ds \\ \oint_{\partial\Omega_N} \partial_{\vec{n}} U(\bar{x}) G(\bar{x}|\bar{x}_0) ds &\approx \sum_{i=1}^{N_N} \partial_{\vec{n}} U(\bar{x}_i) \oint_{\partial\Omega_{N,i}} G(\bar{x}|\bar{x}_0) ds \end{aligned}$$

Taylor expanding about the panel center \bar{x}_{pc} gives an expansion error $h * U'(\bar{x}_{pc})$.

If \bar{x} is on the boundary, then using Eq. (16) calculates the potential from mixed boundaries at interior point \bar{x}_0 as Eq. (17). Note that the flux on Dirichlet and the potential on Neumann boundaries is unknown and needs to be solved.

$$\begin{aligned} \frac{U(\bar{x}_0)}{2} = & \sum_{i=1}^{N_D} U(\bar{x}_i) \oint_{\partial\Omega_{D,i}} \partial_n G(\bar{x}|\bar{x}_0) ds + \oint_{\partial\Omega_N} U(\bar{x}) \partial_{\vec{n}} G(\bar{x}|\bar{x}_0) ds \\ & - \sum_{i=1}^{N_N} \partial_{\vec{n}} U(\bar{x}_i) \oint_{\partial\Omega_{N,i}} G(\bar{x}|\bar{x}_0) ds - \oint_{\partial\Omega_N} \partial_{\vec{n}} U(\bar{x}) G(\bar{x}|\bar{x}_0) ds \end{aligned} \quad (17)$$

In the above formulation, $\partial_{\vec{n}} U(\bar{x})|_{\partial\Omega_D}$ and $U(\bar{x})|_{\partial\Omega_N}$ are required. To reduce the order of the problem, first examine the \bar{x}_1 Dirichlet nodes in the edges around the boundary \bar{x} . As a function of separation between points, the Green's functions can always be calculated around the boundary \bar{x} , leaving the desired unknowns and the given $\check{\gamma}$

$$\sum_{i=1}^{N_D} \partial_{\vec{n}} U(\bar{x}_i) \oint_{\partial\Omega_i} G(\bar{x}|\bar{x}_1) ds - \sum_{i=1}^{N_N} U(\bar{x}_i) \oint_{\partial\Omega_i} \partial_{\vec{n}} G(\bar{x}|\bar{x}_1) ds = \check{\gamma}(\bar{x}_1) \quad (18)$$

where $\check{\gamma}(\bar{x}_1)$ are the known values given by

$$\check{\gamma}(\bar{x}_1) = -\frac{U(\bar{x}_1)}{2} + \sum_{i=1}^{N_D} U(\bar{x}_i) \oint_{\partial\Omega_i} \partial_{\vec{n}} G(\bar{x}|\bar{x}_1) ds - \sum_{i=1}^{N_N} \partial_{\vec{n}} U(\bar{x}_i) \oint_{\partial\Omega_i} G(\bar{x}|\bar{x}_1) ds \quad (19)$$

Similarly, to solve for the potential on flux boundaries, let \bar{x}_2 be on a Neumann boundary. Then

$$\frac{U(\bar{x}_2)}{2} - \sum_{i=1}^{N_N} U(\bar{x}_i) \oint_{\partial\Omega_i} \partial_{\vec{n}} G(\bar{x}|\bar{x}_2) ds + \sum_{i=1}^{N_D} \partial_{\vec{n}} U(\bar{x}_i) \oint_{\partial\Omega_i} G(\bar{x}|\bar{x}_2) ds = \alpha(\bar{x}_2) \quad (20)$$

where $\alpha(\bar{x}_2)$ are the known values given by

$$\alpha(\bar{x}_2) = \sum_{i=1}^{N_D} U(\bar{x}_i) \oint_{\partial\Omega_i} \partial_{\vec{n}} G(\bar{x}|\bar{x}_2) ds - \sum_{i=1}^{N_N} \partial_{\vec{n}} U(\bar{x}_i) \oint_{\partial\Omega_i} G(\bar{x}|\bar{x}_2) ds \quad (21)$$

The matrix to solve becomes

$$\begin{bmatrix} a_{1,1} \dots a_{1,N_D} & b_{1,1} \dots b_{1,N_N} \\ a_{N_D,1} \dots a_{N_D,N_D} & b_{N_D,1} \dots b_{N_D,N_N} \\ c_{1,1} \dots c_{1,N_D} & d_{1,1} \dots d_{1,N_N} \\ c_{N_N,1} \dots c_{N_N,N_D} & d_{N_N,1} \dots d_{N_N,N_N} \end{bmatrix} \begin{bmatrix} \partial_{\vec{n}} U(\bar{x}_{1,1}) \\ \dots \\ \partial_{\vec{n}} U(\bar{x}_{1,N_D}) \\ U(\bar{x}_{2,1}) \\ \dots \\ U(\bar{x}_{2,N_N}) \end{bmatrix} = \begin{bmatrix} \check{\gamma}(\bar{x}_{1,1}) \\ \dots \\ \check{\gamma}(\bar{x}_{1,N_D}) \\ \alpha(\bar{x}_{2,1}) \\ \dots \\ \alpha(\bar{x}_{2,N_N}) \end{bmatrix} \quad (22)$$

where the values in the matrix are given by Eq. (23).

$$\begin{aligned} a_{i,j} &= \int_{\partial\Omega_D} G(\bar{x}, |\bar{x}_{1,j}) \, ds \\ b_{i,j} &= - \int_{\partial\Omega_N} \partial_{\vec{n}} G(\bar{x}, |\bar{x}_{1,j}) \, ds \\ c_{i,j} &= \int_{\partial\Omega_D} G(\bar{x}, |\bar{x}_{2,j}) \, ds \\ d_{i,j} &= - \int_{\partial\Omega_N} \partial_{\vec{n}} G(\bar{x}, |\bar{x}_{2,j}) \, ds \\ \check{\gamma}(\bar{x}_1) &= -\frac{U(\bar{x}_1)}{2} + \oint_{\partial\Omega_D} U(\bar{x}_i) \partial_{\vec{n}} G(\bar{x}|\bar{x}_1) \, ds - \oint_{\partial\Omega_N} \partial_{\vec{n}} U(\bar{x}_i) G(\bar{x}|\bar{x}_1) \, ds \\ \alpha(\bar{x}_2) &= \oint_{\partial\Omega_D} U(\bar{x}_i) \partial_{\vec{n}} G(\bar{x}|\bar{x}_2) \, ds - \oint_{\partial\Omega_N} \partial_{\vec{n}} U(\bar{x}_i) G(\bar{x}|\bar{x}_2) \, ds \end{aligned} \quad (23)$$

The potential at any arbitrary point in the domain is thus given by summing the contributions from fixed mixed boundaries, as in Eq. (17). Note that each shape is connected independently, so although it is point-to-point calculations for the Green's functions, the panels need to be calculated as the surface of unique areas in space and not the empty intermediate locales.

3. Calculating the electrostatic panel force

One of the main advantages of the BEM is rapidly computing the interface force directly from the problem formulation itself. Solving the matrix Eq. (22) for the $\partial_{\vec{n}} U(\bar{x}_1)|_{\partial\Omega_D}$ term provides the normal component of the electric field (σ) on the surface. Gauss' Law says that the total flux of the electric field through an element is

$$UL = \oint \vec{E} \cdot \vec{n} \, dA = \oint E_n \, dA \quad (24)$$

This field comes from the total interior charge Q_{inside} , so the net potential is $UL = E_n L \cdot 1 = \frac{q}{\epsilon_0}$. Solving for the charge, $q = \epsilon_0 E_n L$. Drawing a box around each panel, Gauss's law requires all flux is out of the surface normal. Therefore, the entire contribution of potential comes from the normal electric field times the panel length, L. Therefore, the total force per unit area experienced on the panel is given by:

$$\frac{\check{F}}{A} = \frac{qE_n}{L \cdot 1} = \epsilon_0 E_n^2 \quad (25)$$

This \check{F} is the desired interface force qE_n from Eq. (4) we were originally looking for, calculated exactly without a surrounding volume grid. It holds for any complex geometry and shape curves.

For typical FEED tip electric field values of $4 \frac{V}{nm}$, the force is approximately 10,000 N. The internally-generated field is determined by $q = 4\pi r_d^2 \epsilon_0 E_{int}$.³¹ Assuming the Rayleigh charge limit, the internal field for a $10 \mu m$ radius droplet is $1.6 \times 10^8 \frac{V}{m}$ and trends as $\frac{5.0 \times 10^5}{\sqrt{r_d}} \frac{V}{m}$.

V. Results

The base computational case is a two dimensional field emitter with indium as a propellant and ring electrodes surrounding the tip. Indium has a viscosity of $1.17 \times 10^{-3} \frac{N \cdot s}{m^2}$, surface tension of $0.552 \frac{N}{m}$ and an electric field at the tip of $130 \frac{V}{nm}$. As the simulation is a 2D planar slice instead of a full ring electrode surrounding the emitting needle, the electrostatic force comes largely from 2 points at the edges of the electrode instead of equally surrounding the needle tip. This results in unrealistic 2D force vectors. If setup in a 2D axisymmetric formulation, the resulting electric field is thirty times greater. Simulation run time

for a 256x1024 level set rectangular grid with 1,400 boundary panels is a few hours on a 3 GHz machine. If the matrix in Eq. (22) is solved with iterative GMRes or fast multipole methods, the solution is calculated approximately 8% more rapidly.

Using Eq. (25), the force on the surface can be calculated and then advected forward in time with Eqs. (1, 7 and 9). Indium FEEP droplets are formed as a function of space and time, as seen in the following figures. Figure (4a) shows the fluid traveling at $570 \frac{m}{s}$. The black circle encloses a droplet right before pinching off. An underlying coarse grid is visible in Fig. (4b). The size and charge:area ratios at snap-off come from these panels via the methods of Sec. 3. Several droplet charge/mass examples for various evolution properties are presented in Table 1. If the area was represented as a cross section of a sphere, the droplet mass is indicated by the last column.

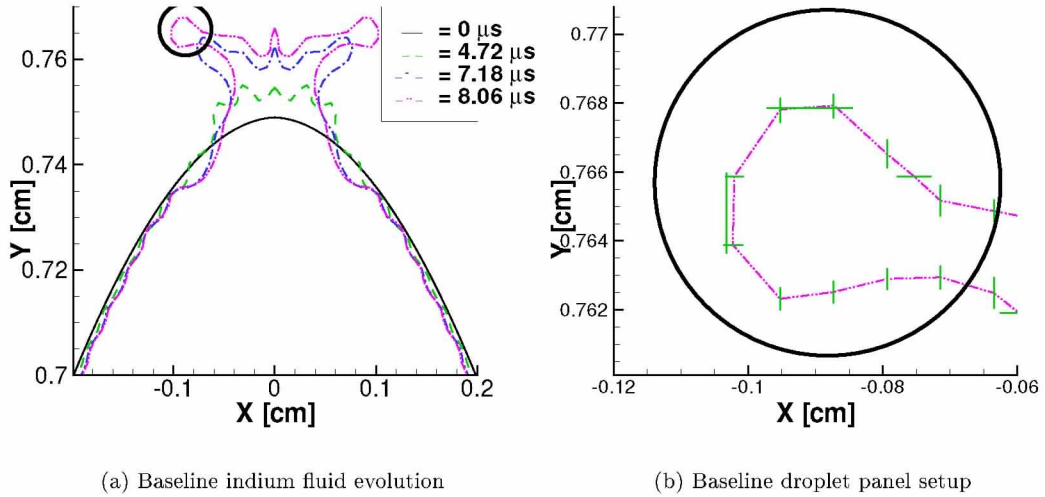


Figure 4. Baseline droplet formation case

Case	Charge [q]	Area [cm^2]	$\frac{Charge}{Area} [\frac{C}{m^2}]$	Droplet Mass [kg]
base	6.80×10^{15}	1.05×10^{-5}	1.04×10^6	1.79×10^{-10}
$\downarrow \mu$	1.98×10^{17}	2.07×10^{-4}	1.534×10^6	1.57×10^{-8}
$\uparrow \gamma$	3.91×10^{15}	8.03×10^{-6}	7.80×10^5	1.20×10^{-10}
\leftrightarrow electrode	4.67×10^{16}	1.48×10^{-6}	5.05×10^7	9.49×10^{-12}
$\downarrow U$	5.37×10^{15}	3.44×10^{-5}	2.50×10^5	1.06×10^{-9}

Table 1. Droplet charge and area scenarios

The viscosity, surface tension, electrode spacing and potential are varied by an order of magnitude. Visual comparisons and descriptions follow.

A. Viscosity

As the fluid viscosity changes, the corresponding shape deformation varies. With low viscosities of Fig. (5b) the indium rapidly moves along the surface of the underlying needle. The transmission of the boundary waves progresses down the entire tip in less than three microseconds. Multiple emission sites form on the tip and begin to detach and emit droplets faster and more thoroughly than in any other situation. Note the tremendous amount of charge on the forming blobs and the largest area of separation.

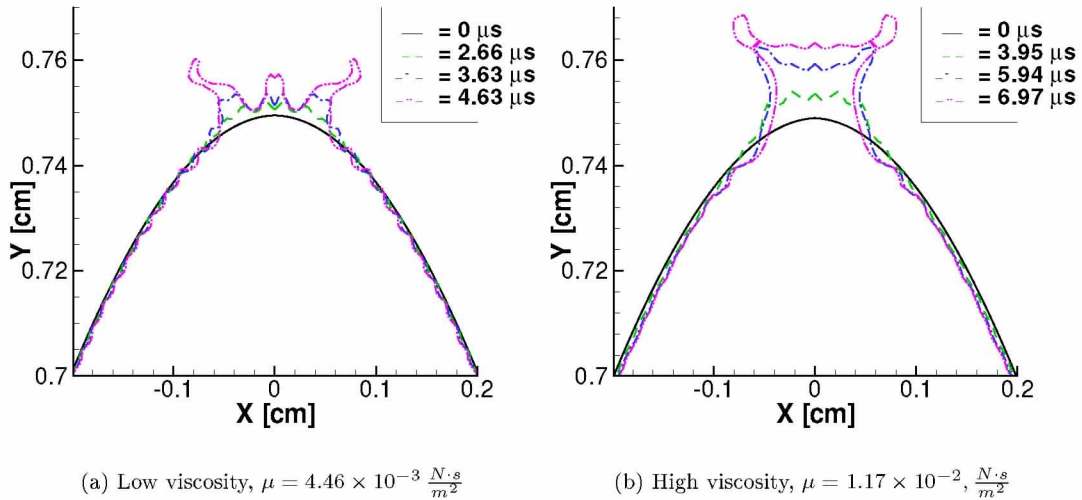


Figure 5. Effect of viscosity on droplet evolution

B. Surface Tension

The evolving surface changes when the liquid possesses an order of magnitude larger surface tension. Here, the force resisting detachment is larger, as the tendency to pull together larger volumes of liquid is greater. This can be seen in the large area of the new droplet in Table 1 and in Fig. (6b). However, the most noteworthy aspect is the small surface charge density as the boundary:surface ratio increases for more massive detachment. The droplets form at a later time, as the formation is retarded due to the larger restraining force at each time step. Note also that the ripples along the needle surface are markedly reduced, another consequence of the smoothing effects of increased surface tension.

C. Size of axial gap

Moving the electrodes three times further from the centerline compared to the base case of Fig. (2) results in a relatively larger horizontal force. Combined with a larger potential flow, the tendrils in Fig. (7b) are pulled out further, faster and finer compared to the base case.

D. Electric field

A lower electric field has the expected value of increasing the time of droplet formation and pulling more of the blob along with it, due to the greater amount of surface relaxation during evolution. Higher specific impulses come from greater charges, with the acceleration of Fig. (8a) as $7.8 \times 10^6 \frac{m}{s^2}$, 1.7 times greater than the lower potential case depicted in Fig. (8b).

VI. Conclusion

The coupling of the boundary element and level set methods allows for the simulation of liquid indium forming a droplet off a field emitter tip. The boundary element method provides a rapid calculation of the external potentials and normal electric fields, thereby driving the propellant's evolution. Due to the surface-only character of the BEM, an arbitrary and complex shape is allowed and the normal electric field calculated on it. Electrostatic potential forces are then coupled into the level set ϕ updating. The combination of the two methods provides an accurate simulation of a two dimensional electrode forming droplets. The qualitative

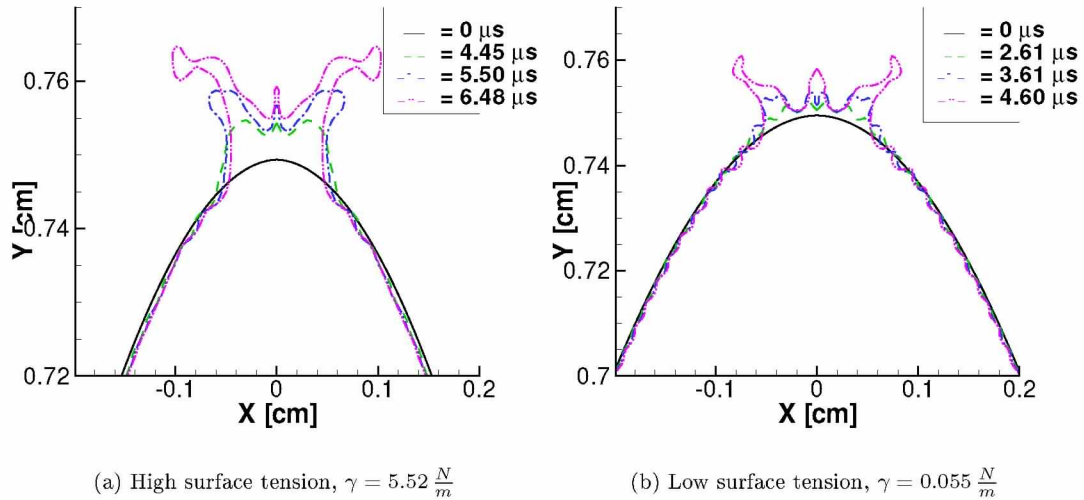


Figure 6. Effect of surface tension on droplet evolution

effects of varying viscosity, surface tension, size of axial gap and electrode potential were investigated.

In on-going work, the 2D planar droplet formulation is being expanded where droplet sizes and charges will be modeled after breakoff. This is possible due to the treatment of each shape as an independent surface and not requiring the continuous connection through a detached droplet.

Acknowledgments

The first author thanks the NASA Jet Propulsion Laboratory for funding through the NASA Graduate Student Research Program.

References

- ¹Genovese, A., Steiger, W., and Tajmar, M., "Indium FEEP Microthruster: Experimental Characterization in the 1-100 μ N Range," Vol. AIAA 2001-3788 of *37th Joint Propulsion Conference*, 8-11 July 2001, pp. 1-12.
- ²Genovese, A., Tajmar, M., and Steiger, W., "Indium FEEP Endurance Test: Preliminary Results," No. IEPC-01-289 in IEPC 27th International Electric Propulsion Conference, Pasadena, CA, October 2001.
- ³Tajmar, M. and Genovese, A., "Experimental evaluation of a mass-efficiency model for an indium liquid-metal ion source," *Journal Physics A*, Vol. 76, 2003, pp. 1003-1006.
- ⁴Vladimirov, V. and Gorshkov, V., "Stability of conducting beams in ionic sources on liquid metals," *Journal of Technical Physics*, Vol. 57, No. 11, 1987, pp. 2155-2163.
- ⁵Taylor, G., *Proceedings of the Royal Society of London*, Vol. A120, 1964, pp. 383.
- ⁶Swanson, L., "Electron and ion emission from liquid metal surfaces," *IEEE Transactions on Plasma Science*, Vol. 19, No. 5, Oct. 1991, pp. 746-748.
- ⁷Kang, N. and Swanson, L., *Applied Physics*, Vol. A30, 1983, pp. 95.
- ⁸Rudenaer, F., Fehring, M., and Steiger, W., "Indium field emission microthrusters," No. SP-398 in Proceedings of the Second European Spacecraft Propulsion Conference, 27 May 1997, pp. 267-271.
- ⁹de Jonge, N., Allieux, M., Doytcheva, M., and Kaiser, M., "Characterization of the field emission properties of individual thin carbon nanotubes," *Applied Physics Letters*, Vol. 85, No. 9, 30 Aug. 2004, pp. 1607-1609.
- ¹⁰Edcombe, C. and Johansen, A., "Current-voltage characteristics of nonplanar cold field emitters," *J. Vac. Science Technology B*, Vol. 21, No. 4, July 2003, pp. 1519-1522.
- ¹¹Chung, M., Miskovsky, N., Cutler, P., Kumar, N., and Patel, V., "Theoretical analysis of a field emission enhanced semiconductor thermoelectric cooler," *Solid-State Electronics*, Vol. 47, No. 10, Oct. 2003, pp. 1745-1751.
- ¹²Forbes, R., "Field electron and ion emission from charged surfaces: a strategic historical review of theoretical concepts," *Ultramicroscopy*, Vol. 95, 200, pp. 1-18.

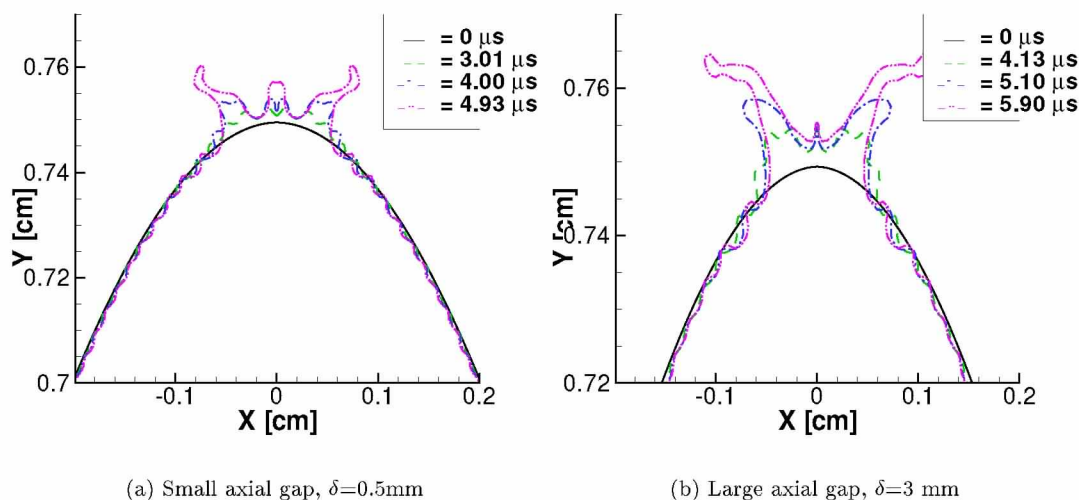


Figure 7. Effect of size of axial gap on droplet evolution

¹³Experimental study of colloid annular thrusters, No. AIAA-70-1112 in 8th Electric Propulsion Conference, Stanford, California, Sept. 1970.

¹⁴Colloid annular array thruster development, No. AIAA-73-1077 in 10th Electric Propulsion Conference, Lake Tahoe, New York, Nov. 1973.

¹⁵Lozano, P. and Martinez-Sanchez, M., "Experimental Measurements of Colloid Thruster Plumes in the Ion-Droplet Mixed Regime," No. 2002-3814 in AIAA 38th Joint Propulsion Conference, Indianapolis, IN, July 2002, pp. 1-7.

¹⁶Nicolini, D., Marcuccio, S., and Andrenucci, M., "3-D Plume Characterization of a FEEP Thruster," No. 2000-3269 in AIAA 36th Joint Propulsion Conference, Centropazio, Huntsville, AL, July 2000, pp. 1-4.

¹⁷Carretero, J. and Martinez-Sanchez, M., "Quasi-one-dimensional numerical simulation of a single-emitter colloidal jet," Vol. AIAA 2002-3812 of 38th Joint Propulsion Conference, Indianapolis, Indiana, 7-10 July 2002, pp. 1-7.

¹⁸Tajmar, M., Steiger, W., and Genovese, A., "Indium FEEP Thruster Beam Diagnostics, Analysis and Simulation," No. 2001-3790 in JPC 37th Joint Propulsion Conference, Austrian Research Centre Seibersdorf, Salt Lake City, UT, July 2001.

¹⁹VanderWyst, A., "Parametric Study of FEEP Mass Efficiency," Tech. rep., University of Michigan, Ann Arbor, Michigan, July 2003.

²⁰Berti, E., Buonanno, A., and Will, C., "Estimating spinning binary parameters and testing alternative theories of gravity with LISA," *Physical Review D*, Vol. 71, No. 8, April 2005.

²¹Kern, M. and et. al., "Outlier detection algorithms and their performance in GOCE gravity field processing," *J. Geodesy*, Vol. 78, No. 9, April 2005, pp. 509-519.

²²Tajmar, M., Genovese, A., Buldrini, N., and Steiger, W., "Miniturized Indium-FEEP Multiemitter Design and Performance," Vol. AIAA 2002-5718, AIAA NanoTech 2002, Houston, TX, 9 September 2002, pp. 1-7.

²³Farag, A. and Hassan, H., "Adaptive Segmentation of Multi-model 3D Data Using Robust Level Set Techniques," *MICCAI LNCS*, Vol. 3216, 2004, pp. 143-150.

²⁴Cookson Electronics, "Technical bulletin:indium...minor metal, major impact," Tech. rep., www.alphametals.com, Jersey City, NJ, 2003.

²⁵Nave, C., "Modeling the radiative cooling of a hot sphere," Tech. rep., Department of Physics and Astronomy, Georgia State University, <http://hyperphysics.phy-astr.gsu.edu/hbase/thermo/cootime.html#c2>, 2005.

²⁶Gibou, F., Fedkiw, R., Cheng, L., and Kang, M., "A second-order-accurate symmetric discretization of the Poisson equation on irregular domains," *J. Computational Physics*, Vol. 176, No. 1, 10 Feb. 2002, pp. 205-227.

²⁷Sussman, M., "A second order coupled level set and volume-of-fluid method for computing growth and collapse of vapor bubbles," *J. Computational Physics*, Vol. 187, 2003, pp. 110-136.

²⁸Rider, W. and Kothe, D., "Reconstructing volume tracking," *J. Computational Physics*, Vol. 141, No. CP985906, 1998, pp. 112-152.

²⁹Sussman, M., Smereka, P., and Osher, S., "A level set approach for computing solutions to incompressible two-phase flow," *J. Computational Physics*, Vol. 114, 1994, pp. 146-159.

³⁰Folland, G., *Introduction to Partial Differential Equations*, Princeton University Press, 1979.

³¹Keidar, M., Beilis, I., Boxman, R., and Goldsmith, S., "Nonstationary macroparticle charging in an arc plasma jet," *IEEE Transactions on Plasma Science*, Vol. 23, No. 6, Dec. 1995, pp. 902-908.

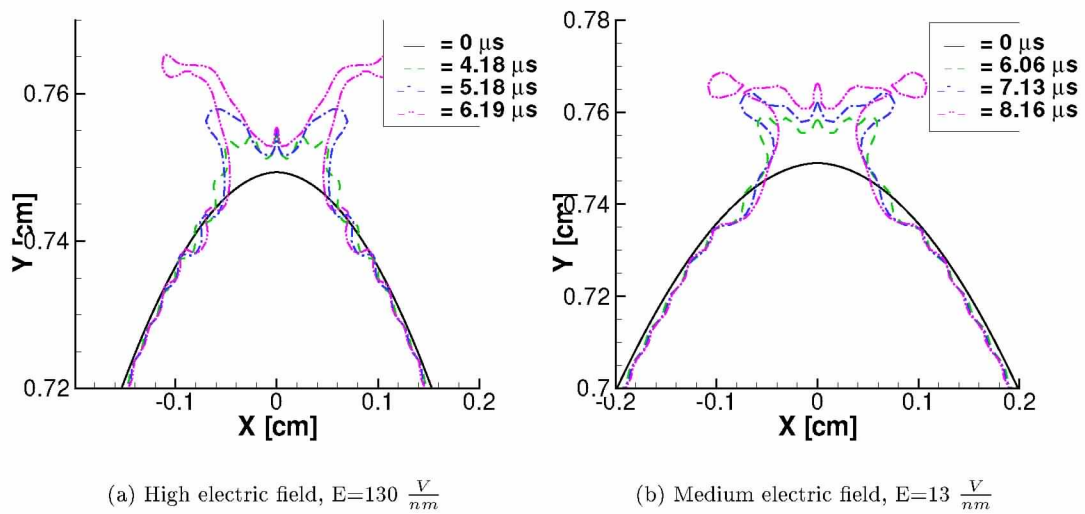


Figure 8. Effect of electric field on droplet evolution